Project of Strategic Interest NEXTDATA

Deliverable D1.3.3
Report on Atmospheric Forcing, Model Calibration and Data Assimilation of the Mediterranean Sea Reconstruction/Reanalysis System (RR)

WP Coordinator: Nadia Pinardi
INGV, Bologna

Authors:
S. Simoncelli, C.Fratianni, N.Pinardi
INGV, Bologna

Summary

Introduction

During the second year of the project a final assessment of the AMIP atmospheric data has been concluded and a localization technique has been implemented within the data assimilation scheme.

The NextData Reconstruction-Reanalysis (RR) of the Mediterranean Sea began production at 1/16 degree resolution, covering a period of sixty years from 1953 to 2012 in the framework of the NextData Project. The first 20 years of the NextData RR have been produced and validated and the results are presented in D1.3.4.

Activities during the second year of the project involved:

- the assessment of AMIP atmospheric forcing and collection of complementary data sets;
- the improvement of the data assimilation scheme *OceanVar*;
- the beginning of RR production covering a sixty year time period.

Atmospheric Forcing analysis

One of the main issues in the NextData RR implementation was the choice of the atmospheric forcing data set, which should include theentire RR time period proposed (1953-2012).

We took into consideration the quality of the AMIP forcing data (Gates, 1992) in order to cover the entire period of study. AMIP data (Cherchi and Navarra, 2007) are available from 1900 up to 2003, and were created through a set of experiments performed with the ECHAM4 atmospheric AGCM on a T126 grid (1.125° of horizontal resolution) forced by HadISST1 (Rayner et al., 2003). AMIP data have a 12 hour temporal resolution. Seven different AMIP realizations were considered, each of them different only by the initial conditions at year 1900. The considered AMIP members are:

- ampt106-1
- ampt106-2
- ampt106-7a
- ampt106-7o
- ampt106-9a

The assessment strategy involved comparing the AMIP data set versus official and well-known ECMWF Reanalysis products: ERA-40 (Uppala et al., 2005; Pettenuzzo et al., 2010) and ERA-Interim (Dee et al., 2011). Tab. 1 summarizes the three data sets analyzed.

Name	Source	Time range	Assimilation	Space resolution	Time resolution
AMIP	CMCC	1898-2006	None	1.125° x 1.125°	12-hourly fields
ERA-Interim	ECMWF	1979-present	4D-VAR	0.75° x 0.75°	6-hourly fields
ERA-40	ECMWF	1958-2002	3D-VAR	1.125° x 1.125°	6-hourly fields

Tab. 1 - Atmospheric data sets compared and their main characteristics.

In the second phase of AMIP assessment we compared model winds with QuikScat scatterometer data products for years 2000-2003. The QuikScat reprocessed ocean surface winds are retrieved from NOAA/NESDIS:
ftp://podaac.jpl.nasa.gov/OceanWinds/quikscat/preview/L2B12/v3/
Reprocessed data consist of gridded daily wind vectors at a spatial resolution of 0.25° in longitude and in latitude.
In order to assess AMIP precipitation fields we used CMAP (Climate Prediction Center Merged Analysis of Precipitation) data provided by the NOAA/OAR/ESRL PSD at http://www.esrl.noaa.gov/psd/ (Xie and Arkin, 1997) already used in the Mediterranean Forecasting System (Oddo et al., 2009). CMAP data are monthly values at 2.5 degrees of spatial resolution.
Reanalysis air-sea fluxes are computed through bulk formulas (see D1.3.2) which need the following input atmospheric data:

- air temperature at 2 m;
- dew point temperature;
- zonal and meridional wind components at 10 m;
- mean sea level pressure;
- total cloud cover.

The atmospheric forcing assessment involved the intercomparison among the three data sets of Table 1, Quikscat and CMAP data sets of all the listed variables, plus precipitation. Each variable was averaged by area and month, considering only sea points. Monthly time series were examined to assess the inter-annual variability, while the climatology was computed to assess the seasonal cycle.

Fig. 1 presents the mean sea level (MSL) pressure results. Each AMIP member shows a particular MSL interannual variability but the same seasonal cycle, which differ substantially from both ERA-Interim and ERA-40 data sets. The AMIP seasonal cycle is about 10HPa wider than ERA-Interim and ERA-40 data sets, with the highest values during the Winter (maximum in January) and lower values during the Summer (minimum in July and August).

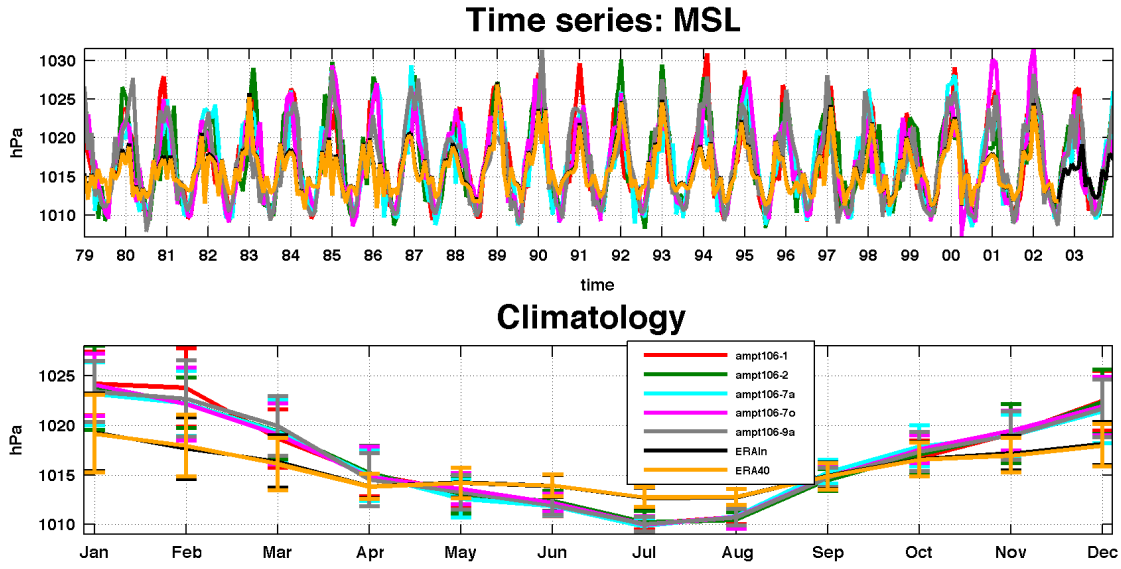

Fig. 1. Mean sea level pressure (MSL) comparison between AMIP members, ERA-Interim and ERA-40 over the 1979-2003 time period: (top) monthly basin average time series; (bottom) monthly climatology.

Figure 2 presents cloud cover (CLC) intercomparison results. Each AMIP member shows approximately the same seasonal cycle which differs from both ERA-Interim and ERA-40 data sets by a value of 5% which is relevant only for the summer. From May to August ERA-Interim and ERA-40 data sets have 5% smaller values than AMIP and this is relevant because the overall CLC value is 10%. AMIP CLC is close to ERA-Interim from January to May, but from June to December AMIP CLC is larger than ERA-Interim.

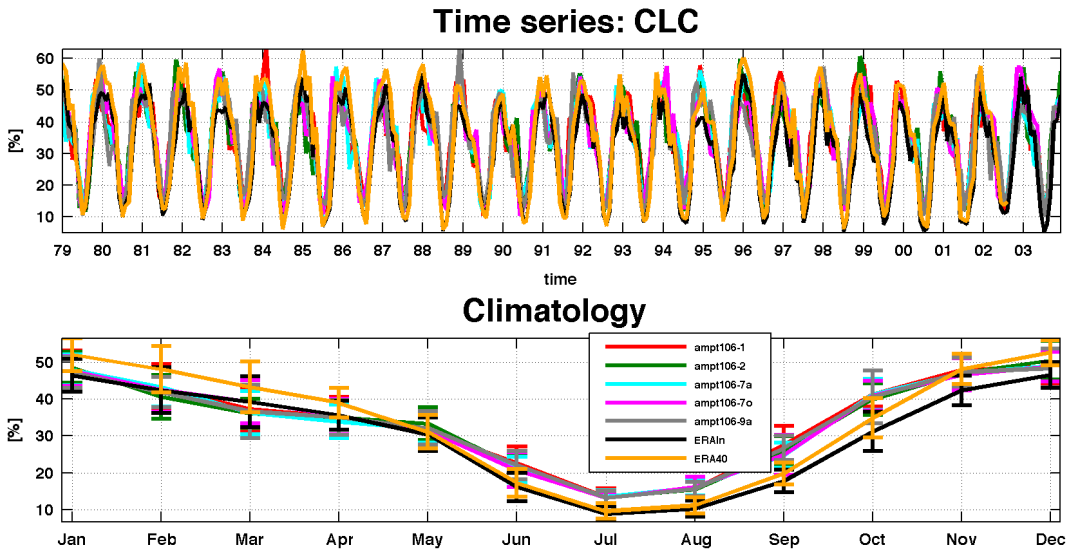

Fig. 2. Cloud Cover comparison between AMIP members, ERA-Interim and ERA-40 over the 1979-2003 time period: (top) monthly basin average time series; (bottom) monthly climatology.

Figure 3 and 4 show the intercomparison of air temperature and dew-point temperatures at 2m. ERA data are very similar for both variables, while all AMIP members show an air temperature close to the ERA values from April to August, and warmer temperatures during the remaining months. AMIP and ERA dew-point temperatures are similar for most of the year: AMIP dew point temperature is slightly warmer in January and slightly colder in June.

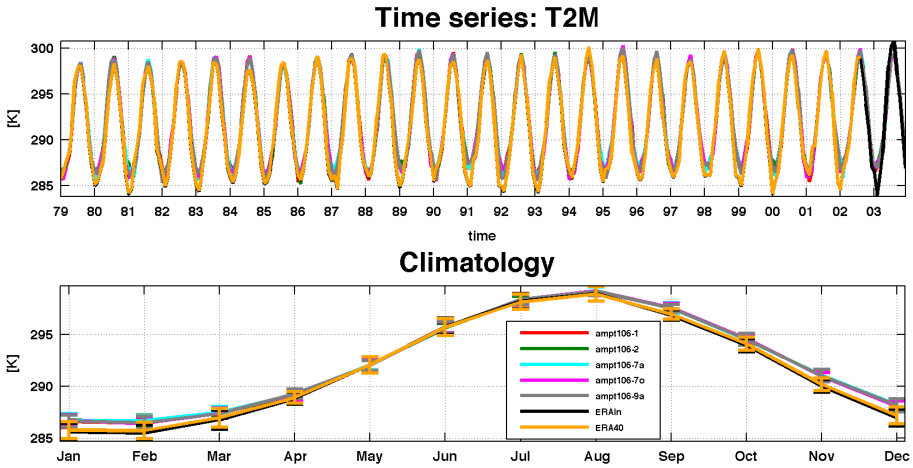

Fig. 3. Comparison of air temperature at 2m (T2M) between AMIP members, ERA-Interim and ERA-40 over the 1979-2003 time period: (top) monthly basin average time series; (bottom) monthly climatology.

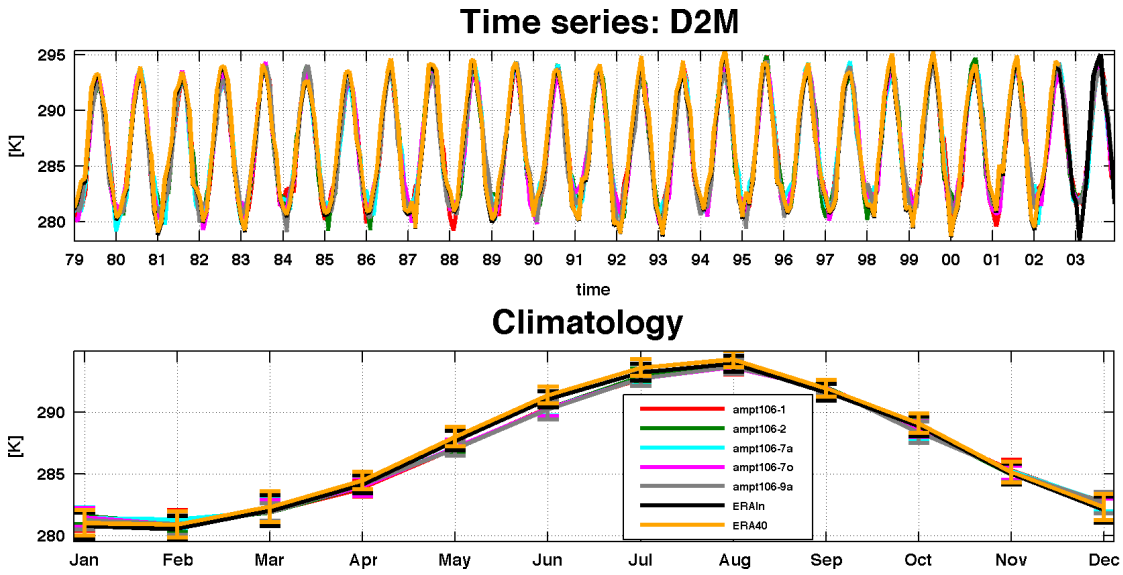

Fig. 4. Comparison of Dew point temperature at 2m (D2M) between AMIP members, ERA-Interim and ERA-40 over the 1979-2003 time period: (top) monthly basin average time series; (bottom) monthly climatology.

Figure 5a-b present *u* and *v* wind components. AMIP zonal and meridional wind components are characterized by larger values and variability than both ERA products. The AMIP meridional wind component shows large negative values indicating that AMIP northerly winds are more intense. Wind intensity in Figure 5c confirms that in winter AMIP have higher values than ERA products with values larger than 8cm/s, while in the summer months, all wind products have values around 4cm/s. AMIP monthly climatology has a wider seasonal cycle and wind intensity is greater than ERA from September to June. ERA-40 display the weakest wind.

Wind products were also validated with satellite observations, using QuickScat data over the years 2000-2003. AMIP and ERA data were horizontally interpolated onto the QuickScat grid and land points were masked before computing the basin average over the Mediterranean Sea. Wind amplitude in Figure 6a highlights that AMIP data agree well with observations in the winter months, while both ERA-Interim and ERA-40 appear too weak. In the summer, QuickScat observations have higher values than both AMIP and ERA products. Observed monthly climatological values (Figure 6b) are greater from June to September. The wind speed frequency plot in Figure 6c highlights that AMIP data match well with the observations, in particular for *amp106-1*, *amp106-2*, and *amp-106-7a.*

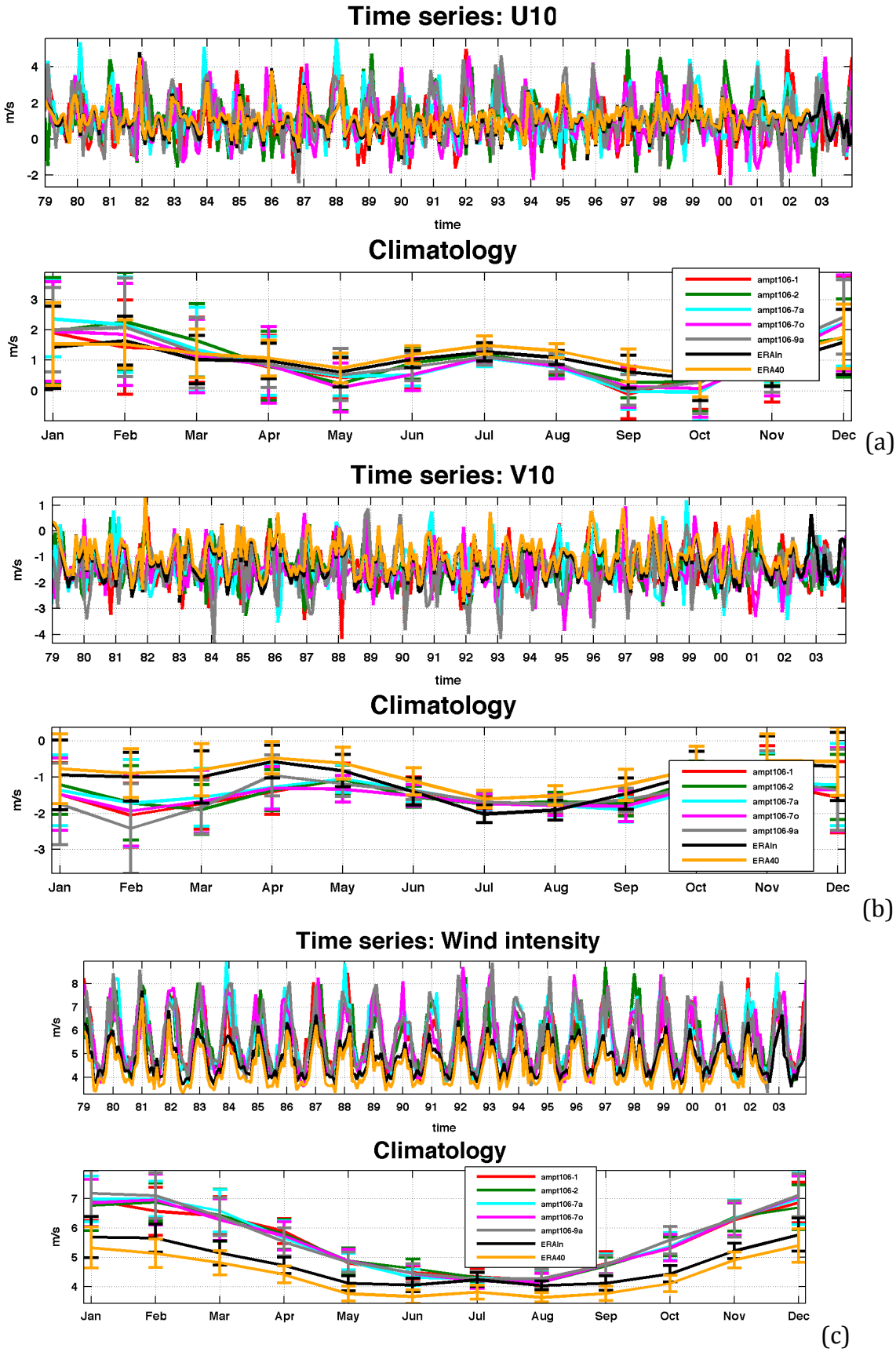

Fig. 5. Comparison of wind at 10m between AMIP members, ERA-Interim and ERA-40 over the 1979-2003 time period: (a) monthly basin average time series and monthly climatology for *u* wind component; (b) monthly basin average time series and monthly climatology for *v* wind component; (c) monthly basin average time series and monthly climatology for wind intensity.

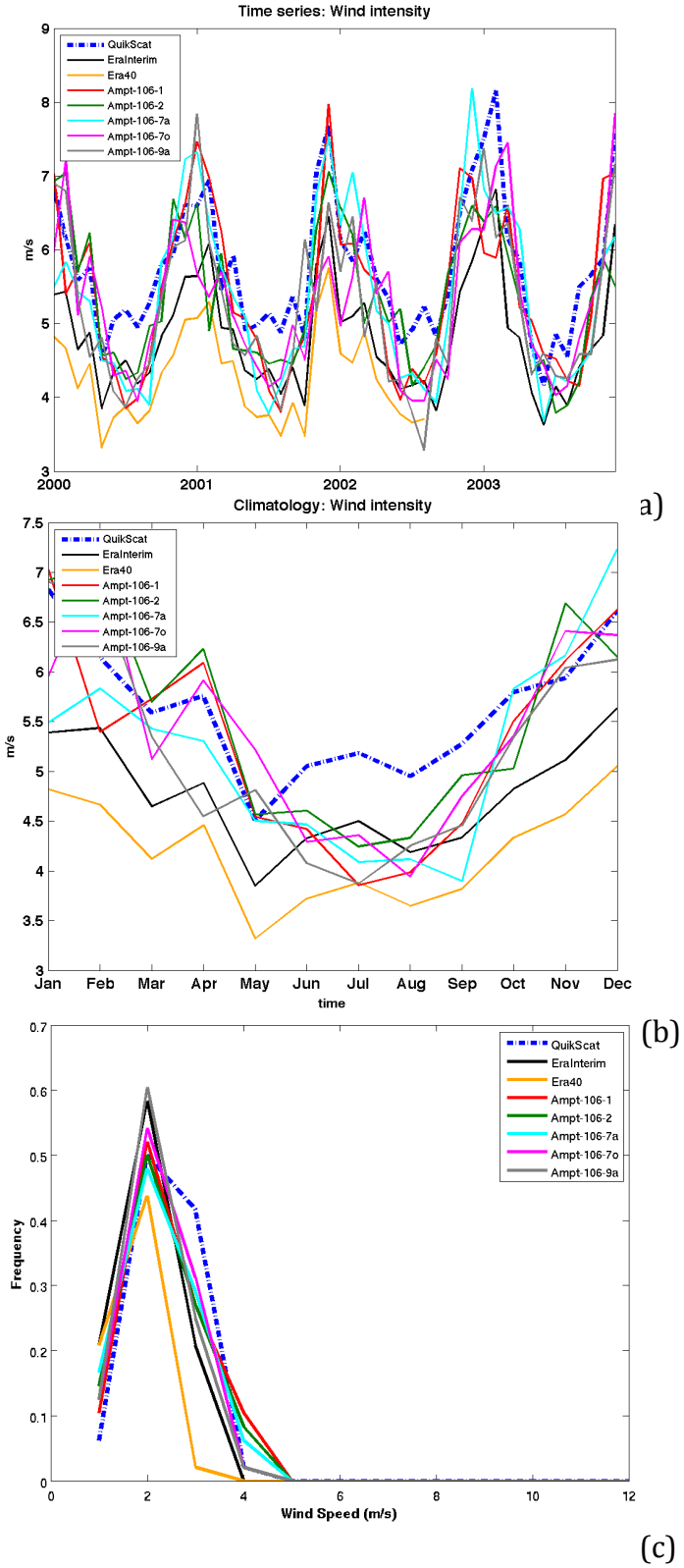

Fig. 6. Validation of AMIP, ERA-Interim and ERA-40 data with QuikScat observations over the time period 2000-2003: (a) monthly basin averaged wind speed time series; (b) wind speed monthly climatology; (c) wind speed frequency diagram.

Figure 7 shows AMIP precipitation compared to ERA data sets. The AMIP data show much higher climatological values than CMAP and ERA-Interim, which instead are in very good

agreement with each other. Both ERA-Interim and CMAP data present values consistent with the literature (Pettenuzzo et al., 2010; Mariotti et al., 2010). We decided to use CMAP monthly climatological data for the NextData RR production.

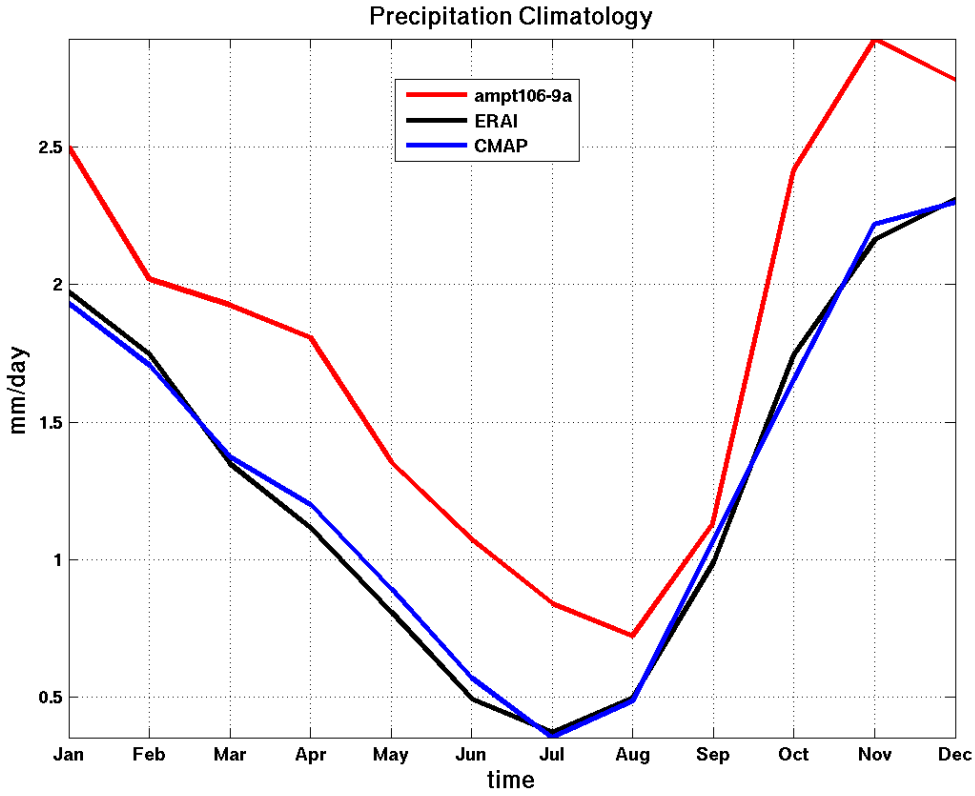

Fig. 7. Monthly climatological precipitations computed for the Mediterranean basin over the time period 1979-2007 for AMIP (amp106-9a), ERA-Interim and CMAP data.

Sea Surface Temperature assessment and correction calibration

The satellite SST is used in the reanalysis to interactively correct the heat flux at the air-sea interface. The heat flux correction is proportional to the difference between the model and the SST observed (Pinardi et al., 2003). Adani et al. (2011) reanalysis systems used Marullo et al. (2007) objectively analysed data set for the period 1985-2007. In order to produce a 60-year NextData RR we had to find another good quality longer period SST dataset. The Met Office Hadley Centre SST dataset (HadSST1) was archived during the first year of the NextData Project. This decision was consistent with using AMIP atmospheric forcing which is also forced by HadSST1. The data set consists of monthly SST on a regular grid of 1°x1° starting from 1870 (Rayner et al., 2003), thus it covers the entire NextData RR time period.

We applied the same approach used for the atmospheric forcing to validate HadSST1 for the Mediterranean Basin, using the best available products in the literature, the Mediterranean SST reconstruction from Marullo et al. (2007), which covers 1985-2008. Table 2 summarizes the main characteristics of the considered datasets.
The first step consisted in assessing a horizontal interpolation method to interpolate HadSST1 onto the RR model grid. We tried both bi-linear and spline horizontal interpolation (Figures 8 and 9). Monthly basin SST time series and related climatologies indicate that spline-interpolation of HadSST1 onto the RR horizontal grid is the best approach to obtain values closer to our reference data set. Figure 9 shows examples (January 1985 and July 2003) of

horizontal monthly SST maps from HadSST1 compared to the reference data set. Horizontal spline-interpolation (middle panels) mimics the horizontal temperature gradient better than bi-linear interpolation (top panels), giving a result closer to our reference data set (bottom panel). It can be concluded that monthly HadSST1 is a good quality SST product for the Mediterranean Sea, characterized by a monthly variability and a monthly climatology close to our reference SST data set.

Name	Source	Time range	Horizontal resolution	Temporal resolution
HadSST1	Met. Office	1950-2012	1° x 1°	Monthly mean
SST reconstruction Marullo et al., 2007	CNR-ISAC	1985-2008	0.0625° x 0.0625°	Daily mean

Tab. 2. Summary of the main characteristics of SST data sets, HadSST1 and SST reconstruction (Marullo et al., 2007) evaluated during the MED RR feasibility study.

Monthly SST maps have to be linearly interpolated in time between adjacent months, assuming that the monthly mean average is applied to day 15 of the month. However, Killworth (1996) pointed out that this procedure does not conserve the monthly average value. To overcome this, Killworth (1996) proposed a simple procedure based on the computation of the so-called "pseudo values" whose linear interpolation preserves the correct average value. We used his technique and the results are displayed in Figure 10. The difference between the original and the corrected data highlights that the correction ranges on basin average between -0.4 and 0.3°C and annual values are preserved. We thus decided to pre-process SST data using a horizontal spline interpolation and Killworth correction.
The last phase of SST assessment focused on the calibration of the relaxation coefficient within the surface temperature boundary condition:

$$\rho_0 C_p (K_H) \left.\frac{\partial T}{\partial z}\right|_{z=\eta} = \left.\frac{dQ}{dT}\right|_{T=T_m} (T_m - T_o)$$

where T_m is the model surface temperature, T_o is the observed SST, and dQ/dT is the restoring coefficient:

$$\frac{dQ}{dT} = \rho_0 C_p \frac{\Delta z}{\Delta \tau}$$

Assuming a $\Delta\tau$ of about 2.5 days and a fixed surface layer thickness (Δz) of 1 m, ad in the RR model, the value is -60W $m^{-2}K^{-1}$ as in *Adani et al.* (2011).

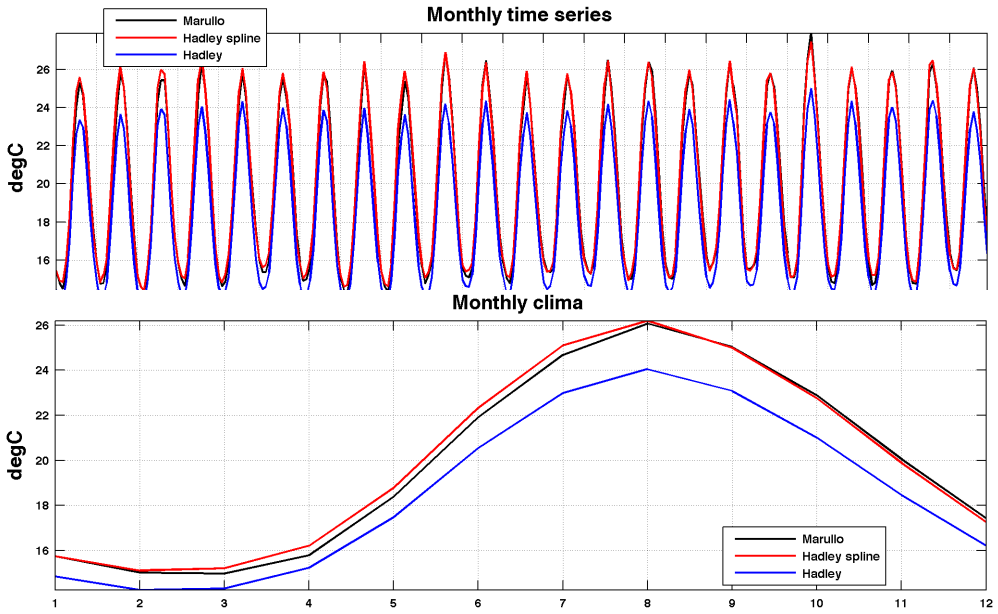

Fig. 2. Mediterranean SST data from Marullo et al. (2007) compared to HadSST1 bi-linear interpolated (red line) or spline interpolated (blue line) onto the RR grid over the time period 1985-2007: (top) monthly basin averages; (bottom) monthly climatologies.

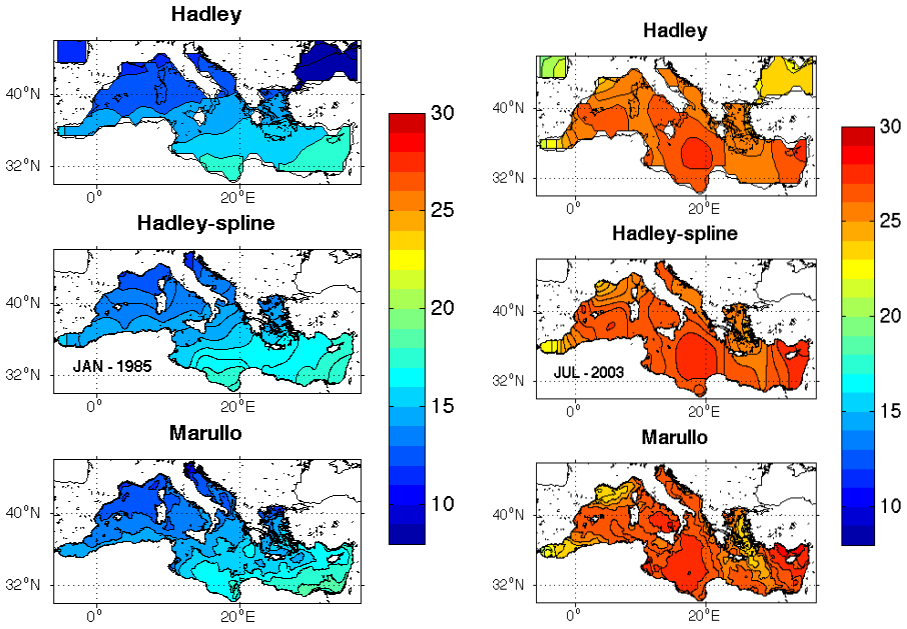

Fig. 3. Monthly SST maps from HadSST1 compared to the reference data set from Marullo et al. (2007): *(left)* January 1985; *(right*) July 2003. Bi-linear interpolated. HadSST1 maps are displayed in the top panels, the middle panels show the result of horizontal spline interpolation, and the bottom panels contain the reference maps.

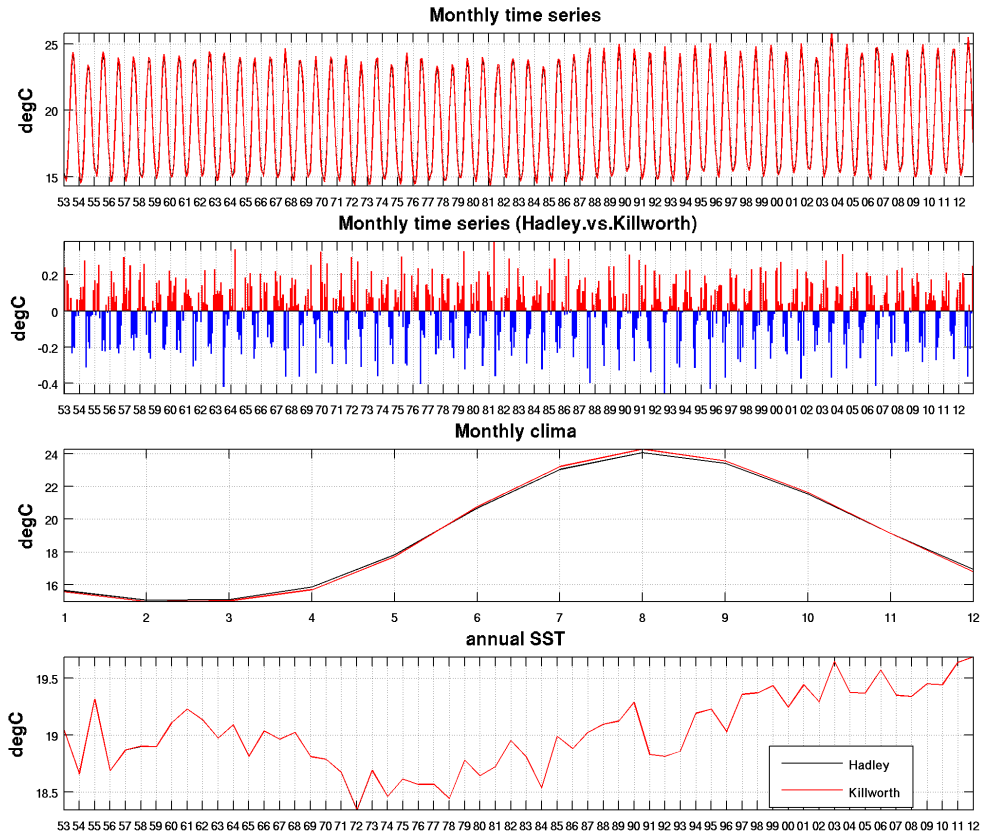

Fig. 10. HadSST1 SST data before and after Killworth correction: (top) monthly time series 1953-2012; (second panel) difference between original HadSST1 and its Killworth correction; (third panel) monthly climatology computed over the entire time period; (bottom) annual mean time series.

Improvement of the Data Assimilation Technique

OceanVar is a three-dimensional variational scheme set up by Dobricic and Pinardi, (2008) which corrects model fields for T, S, sea level and velocity components. The assimilation cycle is daily, as implemented by Adani et al. (2011) and takes into consideration the observations within the 24 hour time interval from 12:00 of day J and 12:00 of day J+1. The correction estimated is applied at model restart at 12:00 on day J+1.

OceanVar calibration analysis was performed during the first year of the project (see D1.3.2) in order to handle an increasing number of observations. Another issue encountered was the sampling pattern of historical observations which are normally given by regularly spaced, finely resolved monitoring arrays or transects.

Many experiments were conducted to calibrate the horizontal correlation length scales in the background error covariance matrix, instrumental error and to improve the horizontal filter which spreads vertical corrections along the horizontal. RR system calibration identified code bugs and defined the method to decrease the correlation length scales implementing a localization technique.

Fig. 4 gives an example of a temperature correction field at a depth of 230 m, when correction overshooting occurred on 30 August, 1987 in the Otranto Strait. Black dots indicate the locations of temperature observations, which are positioned on a transect. As it can be seen, the maximum positive and negative correction values are far from the observation locations due to opposite sign temperature misfits in two close observation positions, as displayed in

the vertical profiles of Figure 12. Our objective was to avoid this kind of unrealistic correction fields and to limit the correction close to the observation location.

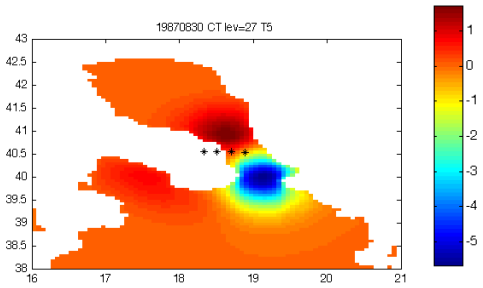

Fig. 4. Temperature correction field in °C at a depth of 230 meters computed by the *OceanVar* scheme.

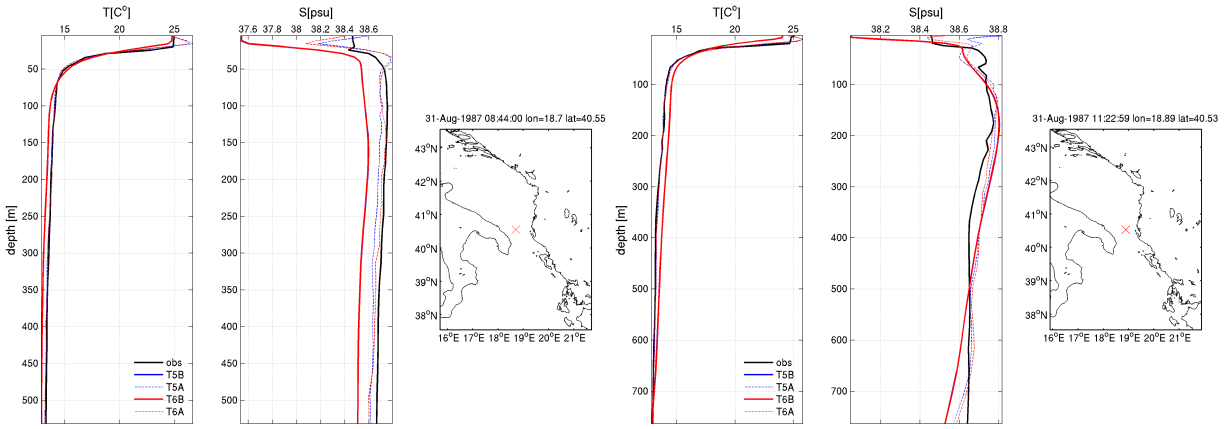

Fig. 12. Two vertical temperature and salinity profiles and their relative space location that were considered by the *OceanVar* assimilation scheme to compute the correction field. The black curves are observations and four experiments are shown: T5 and T6 with both analysis (left) and background fields (right) for each location.

A localization technique was implemented in *OceanVar* code and is based on a vector *l* with the same dimension as the horizontal grid and characterized by values:

- 1 in the four points close to observations;
- 0 in the points far from observations.

Between the two extremes of *l* a Gaussian function is defined:

$$G(r) = e^{-\left(\frac{r^2}{2L_\lambda^2}\right)}$$

with a characteristic radius $R_\lambda = \sqrt{2}L_\lambda$. The *OceanVar* spatial covariance part is computed *(Dobricic and Pinardi 2008)* by the multiplication:

$$B = V_H V_V$$

WhereV_H is the horizontal covariance operator realized by a recursive filter and V_V is the vertical transformation operator. With localization, the error covariance matrix is then defined as:

$$B = \Lambda V_H V_V$$

Where Λ is a diagonal matrix containing the l values. We chose the localization radius R_λ in order to preserve the horizontal covariance in the presence of a single observation, imposing:

$$e^{-\left(\frac{r^2}{R_\lambda^2}\right)} e^{-\left(\frac{r^2}{R_H^2}\right)} = e^{-\left(\frac{r^2}{a^2}\right)}$$

$$\frac{1}{R_\lambda^2} + \frac{1}{R_H^2} = \frac{1}{a^2} \quad , \quad R_\lambda = \sqrt{\frac{a^2 R_H^2}{R_H^2 - a^2}}$$

Where a represents the final correlation length which is kept close to the original *OceanVar* implementation, and R_H is the characteristic length of the horizontal operator V_H. A sensitivity analysis was performed to tune the spatial scales close to the 21 km of the control run experiment (V4bis) which has L_H=15 and R_H=21.2. Table 3 summarizes the sensitivity tests T1, T4 and T6 performed from 30 August to 2 September 1987, when many profiles were available between the southern Adriatic and the northern Ionian basins and from 2-4 January 1995 to check altimeter data.

	L_λ	R_λ	L_H	R_H	a
T1	30	**42.4**	30	**42.4**	30
T4	38.7	**54.7**	21.2	**30**	26.3
T6	30.5	**43.1**	17	**24**	21

Tab. 3. Summary of the sensitivity experiments performed to tune the resulting horizontal covariances spatial scale a. Length scales are expressed in Km.

Figures 13, 14 and 15 show the sea level anomaly, temperature and salinity correction fields respectively, for the control run and the sensitivity experiments of Table 3 on 2 January 1995. The localization technique eliminates spurious signals far from the observation locations, especially in the Ionian Sea. There are no visible differences between the three sensitivity tests results.

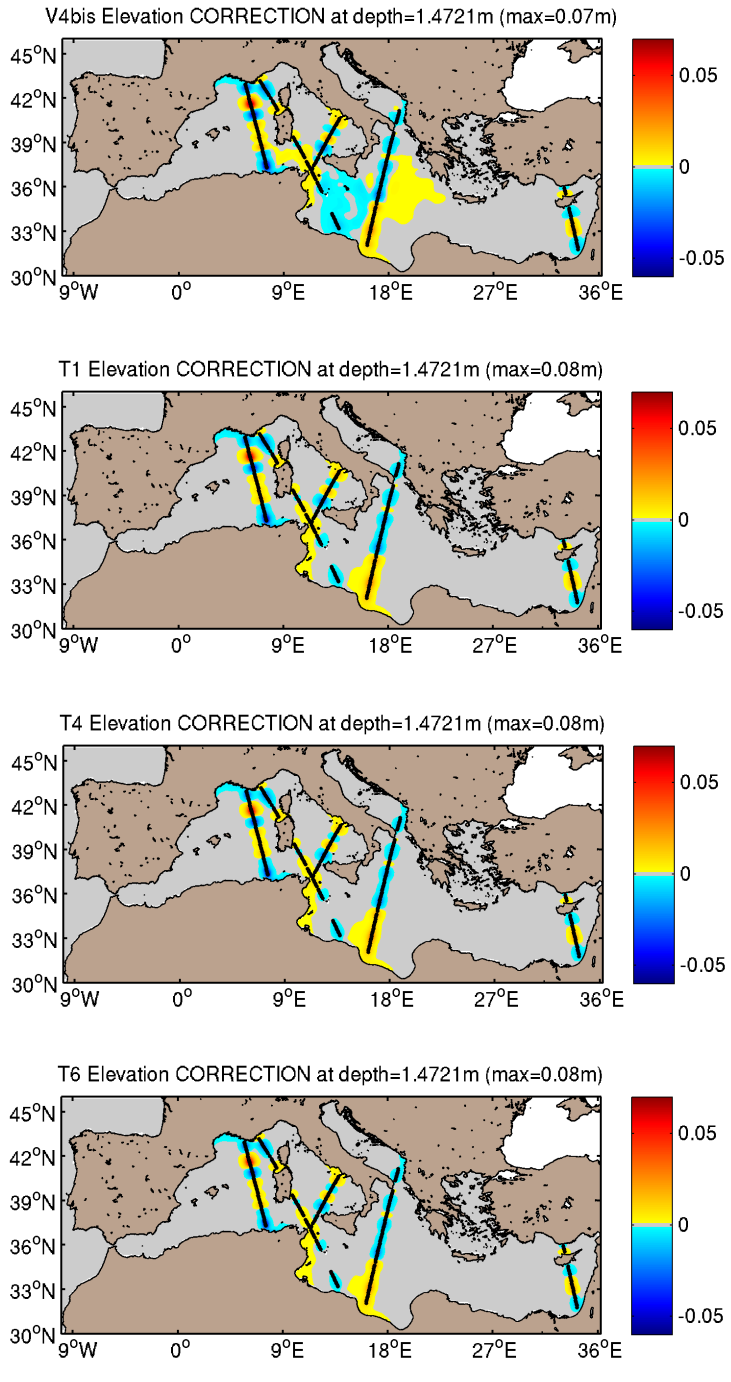

Fig. 13. Sea level anomaly correction field on 2 January 1995: (a) Control run output without localization; (b) T1 experiment result; (c) T4 experiment result; (d) T6 experiment result. Black dots indicate the observation location.

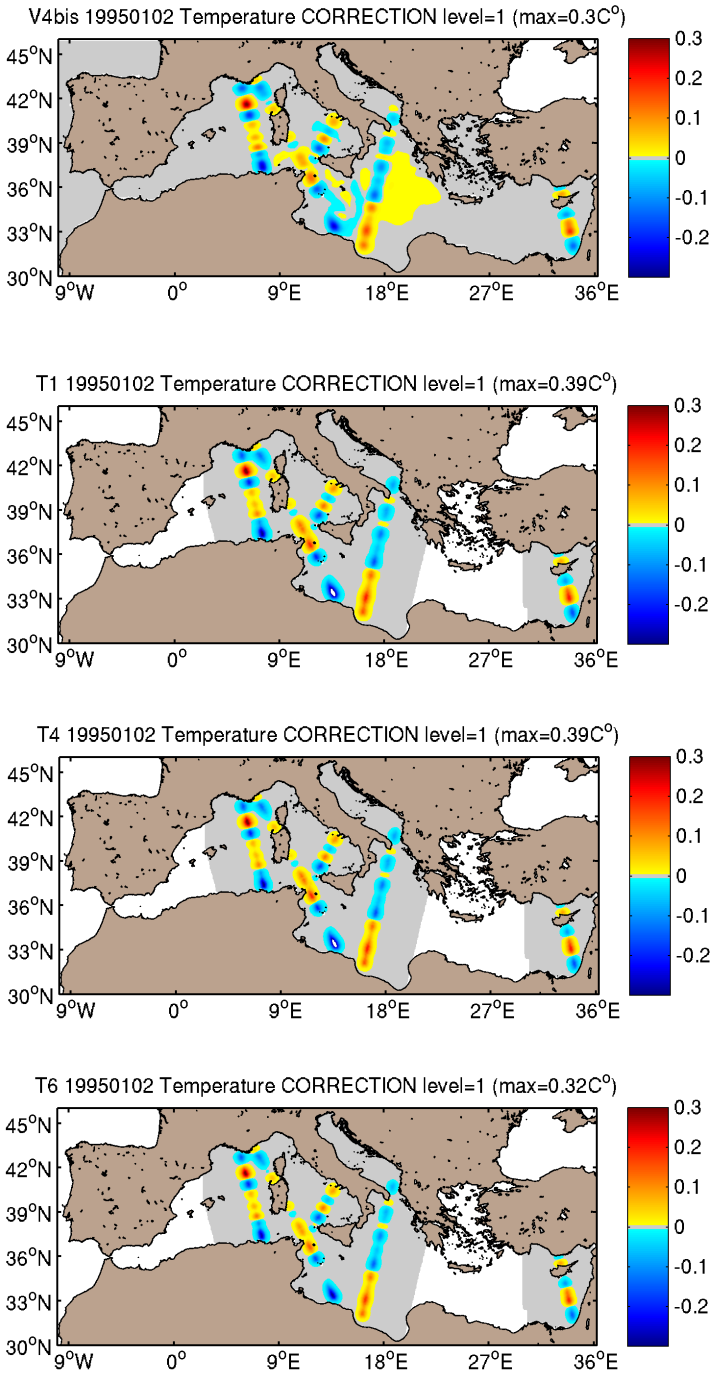

Fig. 14. Temperature correction field on 2 January 1995: (a) Control run output without localization; (b) T1 experiment result; (c) T4 experiment result; (d) T6 experiment result.

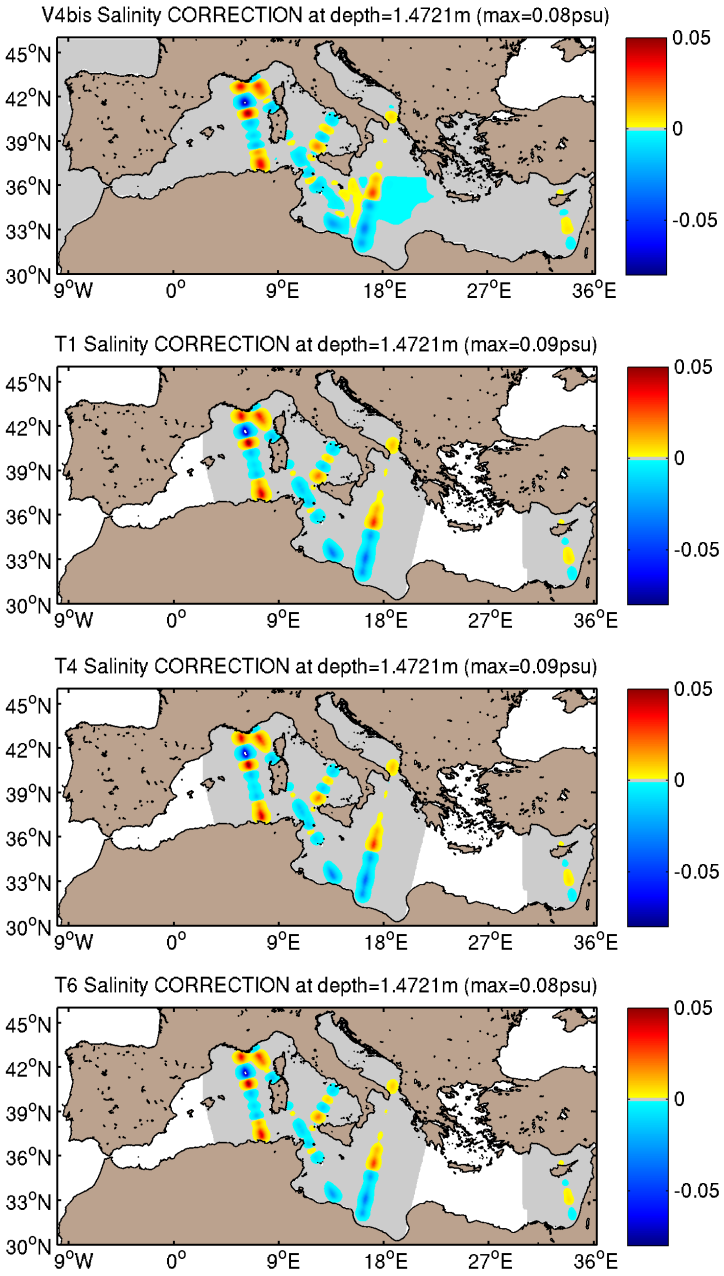

Fig. 15. Salinity correction field on 2 January 1995: a) Control run output without localization; (b) T1 experiment result; (c) T4 experiment result; (d) T6 experiment result.

Figure 16 presents a temperature correction field at a depth of 230 m (cf. Fig. 4) for the control run and sensitivity experiments on 30 August 1987. The localization technique computes different solutions between the three sensitivity tests results and we need to have an objective way to decide which formulation is the best.

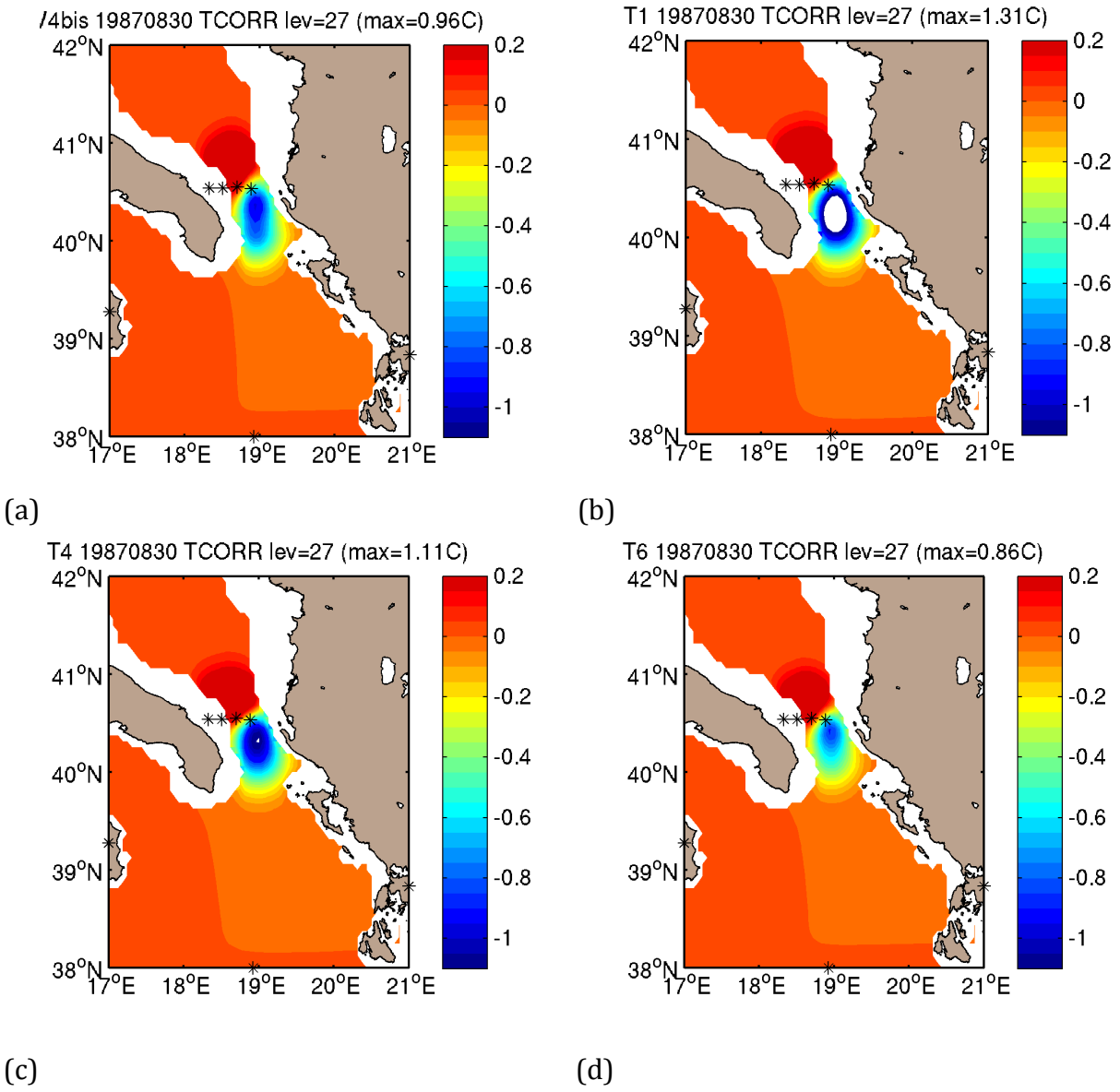

Fig. 16. Temperature correction field at 230 m on August the 30th 1987: (a) Control run output without localization; (b) T1 experiment result; (c) T4 experiment result; (d) T6 experiment result.

In order to quantify the best values for the localization radius we computed the RMSE between model (background) and observations before data assimilation for the period 30 August - 2 September 1987, when observations were available between the southern Adriatic basin and the northern Ionian Sea. The results are displayed in Table 4: although the temperature and salinity RMSE differences are very small, the T6 implementation seems to give the best performance.

RMSE	CTR	T1	T4	T6
TEMPERATURE [C]	1.067	1.067	1.054	1.050
SALINITY [psu]	0.180	0.179	0.174	0.169

Tab. 4. Averaged temperature and salinity RMSE computed from model misfits for temperature and salinity on 31 August, 1 September, and 2 September 1987.

To further test the localization scheme, a numerical experiment was performed in two different periods:

- 1995 to analyze localization results on assimilated altimetry data
- 1985-1987 when three POEM surveys were available.

The results were compared with the control run (V4bis). Here we present the results of the T1 localization implementation only.

Figure 17 reports the daily SLA RMSE time series computed for the year 1995 which show no evident differences in model performance, since on average both experiments present the same RMSE value of 3.5 cm.

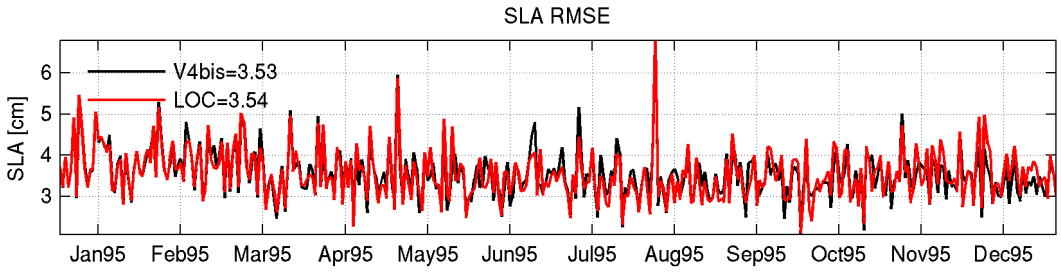

Fig. 17. Daily SLA RMSE [cm] time series computed from misfits before data are assimilated for 1995: (black line V4bis) control run; (red line-LOC) T1 localization experiment.

Figure 18 shows the RMSE and BIAS basin-averaged profiles computed from model misfits for 1995. BIAS average values over the water column differ slightly only for salinity, while salinity RMSE remains the same. Temperature RMSE decreases slightly in the T1 localization experiment. Figure 19 reports BIAS and RMSE basin-averaged profiles computed from model misfits for 1985-1987. Even when a longer time period was considered, model performance was not substantially improved by the localization technique.

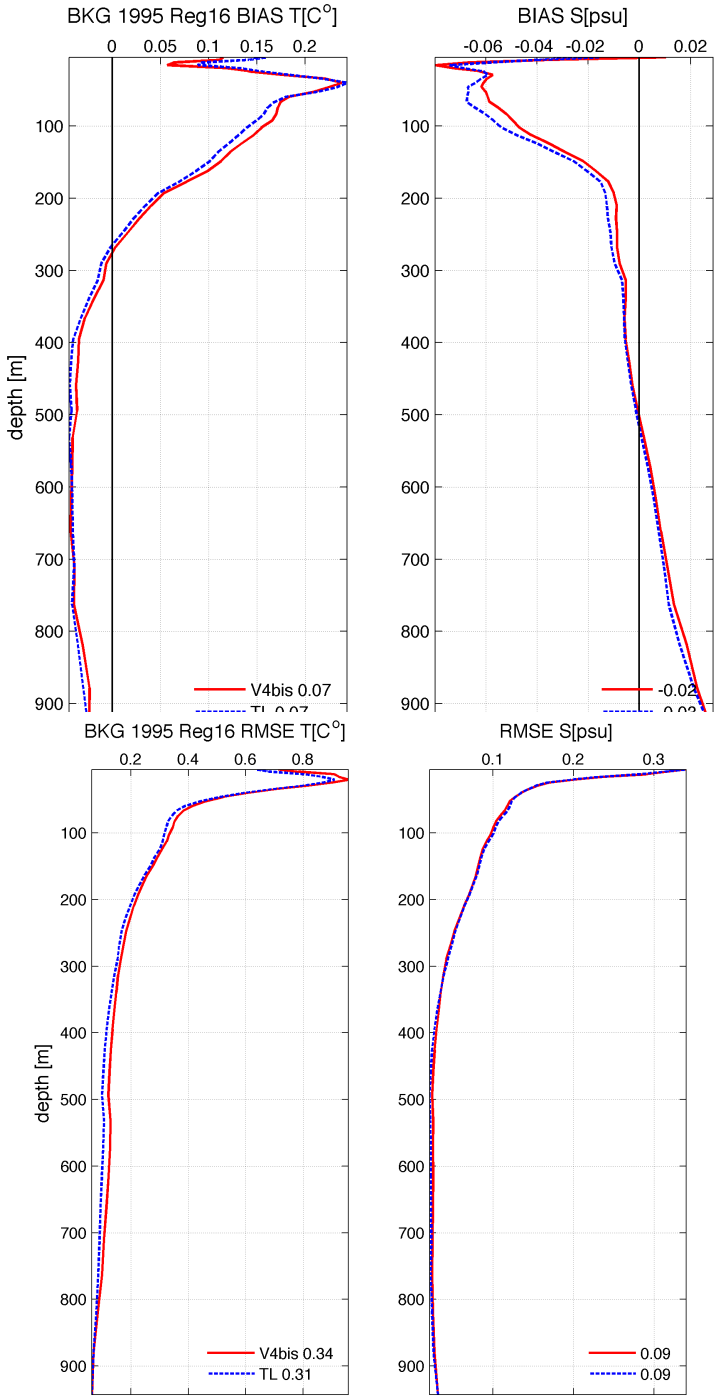

Fig. 18. BIAS (top panels) and RMSE (bottom panels) basin-averaged profiles computed from model misfit for 1995. The red line indicates the control run (V4bis) and the blue line, the localization experiment (T1).

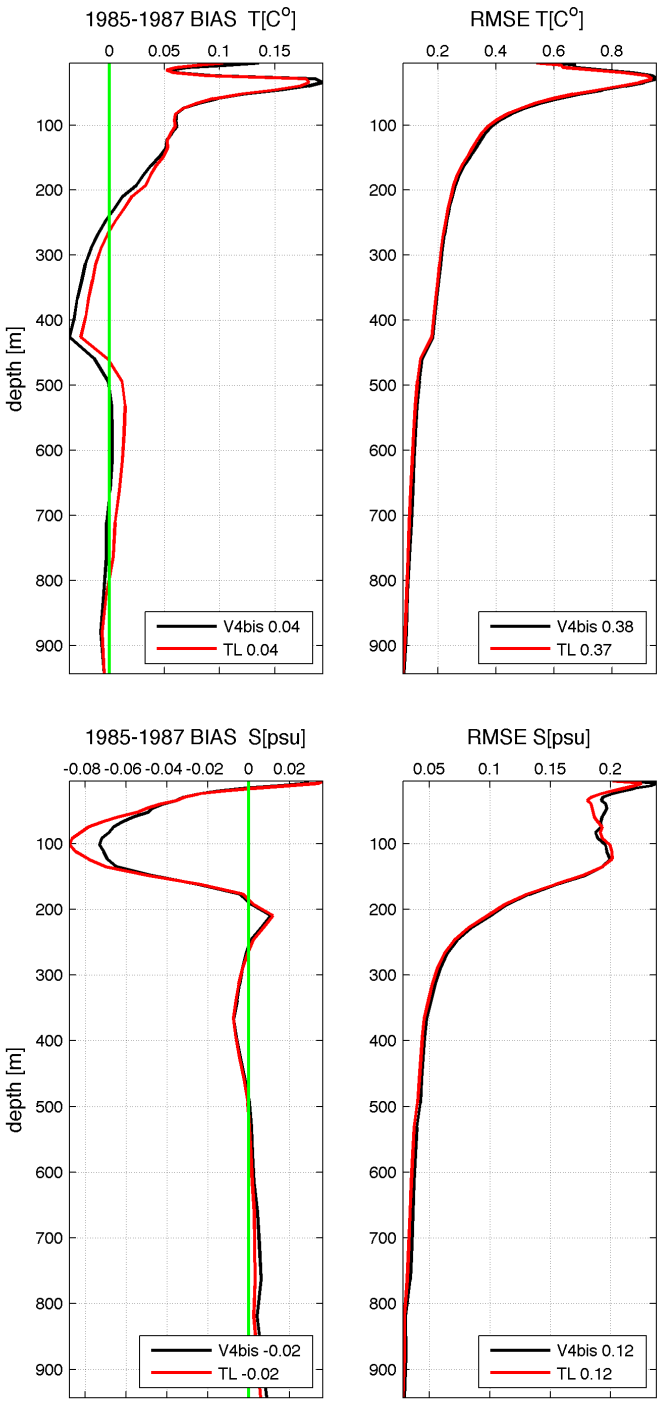

Fig. 19. BIAS (left panels) and RMSE (right panels) basin-averaged profiles computed from model misfits over the time period 1985-1987. The black line indicates the control run (V4bis) and the red line indicates T1 localization experiment. (top) temperature; (bottom) salinity.

In order to show the impact of the localization procedures, we reverted to a local analysis of the circulation structures. Figures 20, 21 and 22 present the monthly mean circulation computed for the control run and the localization experiment T1 in relation to three POEM surveys (Robinson et al., 1991):

- October-November 1985;
- March-April 1986;
- August-September 1987.

In all these cases there are relevant local differences between the control run and the T1, meaning that the localization procedure implements considerable modifications. From this local analysis it is evident for us that the localization gives better results. In November 1985 and April 1986, the Mersa-Matruh Gyre is better located with respect to the literature mapped data, as well as the Rhodes Gyre seems to be more realistic, being more intense along the Asia Minor coasts.

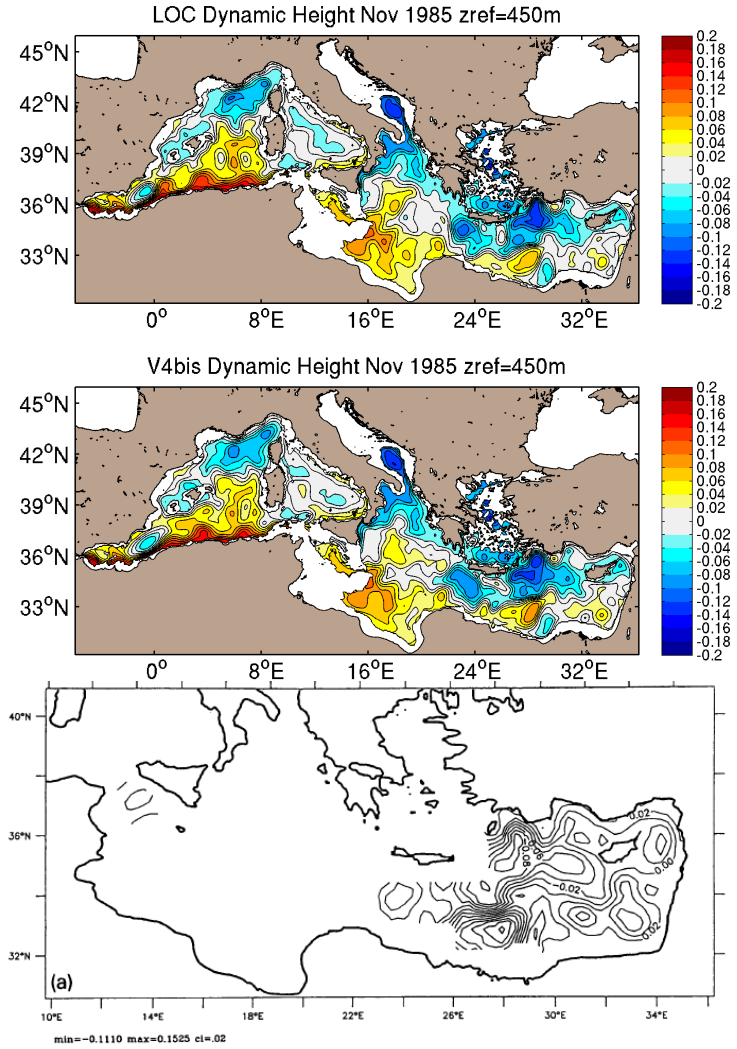

Fig. 20. Monthly circulation computed for the time period corresponding to the POEM experiment of November 1985: (top) T1 localization circulation; (middle) control run V4bis circulation; (bottom) circulation computed from observations from Robinson et al., 1991.

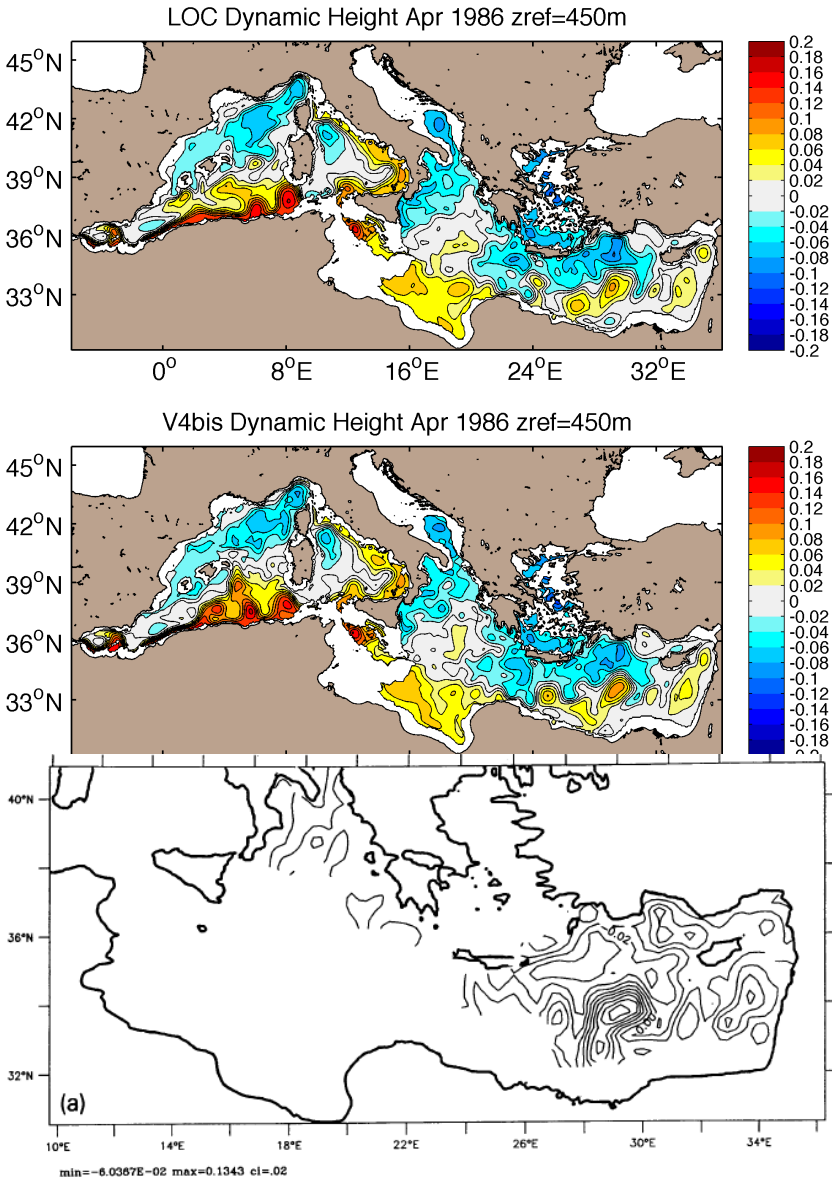

Fig. 21. Monthly circulation computed for the time period corresponding to the POEM experiment of April 1986: (top) T1 localization circulation; (middle) control run V4bis circulation; (bottom) circulation computed from observations from Robinson et al., 1991.

For September 1987 (Figure 22) the Atlantic-Ionian Stream is thinner and stronger, closer to the mapped one, as well as the Rhodes Gyre is larger and more intense in the area of the Anaxymander High.

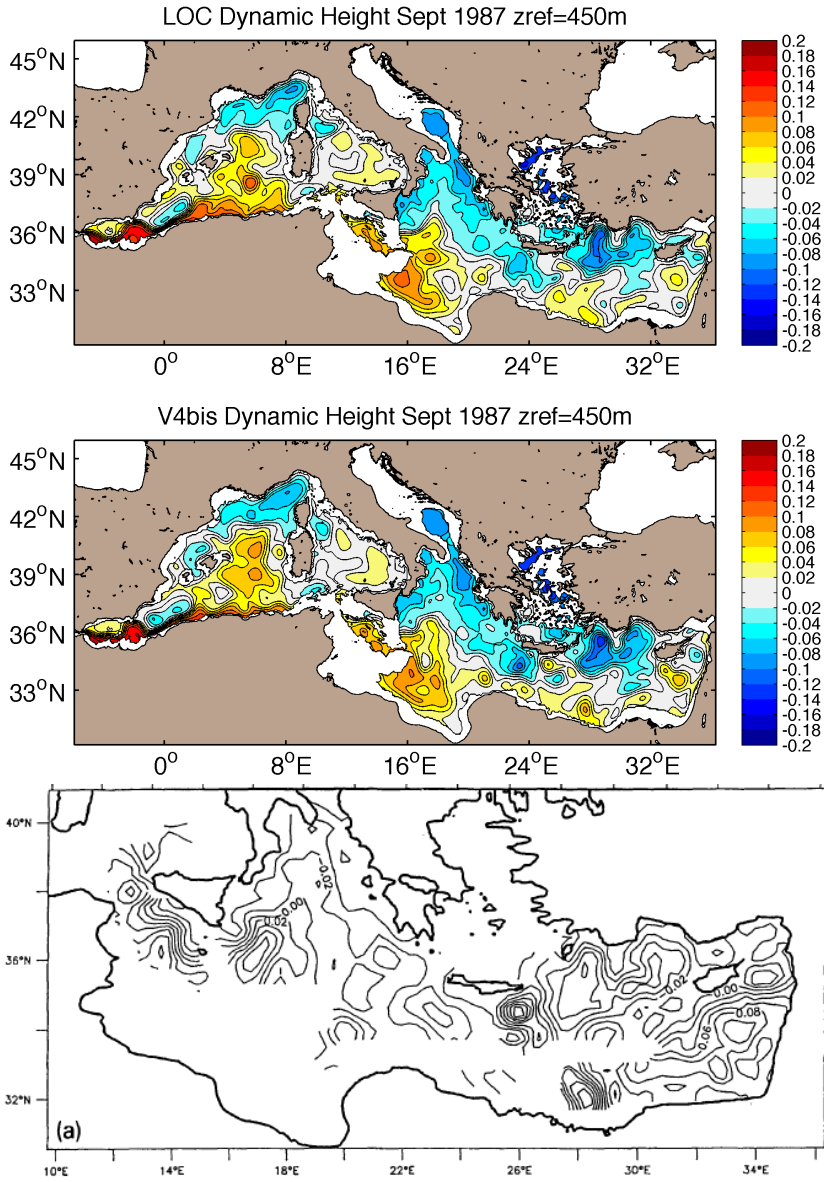

Fig. 22. Monthly circulation computed for the time period corresponding to the POEM experiment of September 1987: (top) T1 localization circulation; (middle) control run V4bis circulation; (bottom) circulation computed from observations from Robinson et al., 1991.

Summary and conclusions

During the second year of WP1.3 activities, all expected results were achieved. The atmospheric forcing was validated and amp106-9a AMIP member was chosen for the NextData RR production, as described in D1.3.4.The AMIP atmospheric variables were assessed by an intercomparison with reanalysis products ERA-40 and ERA-Interim. Winds were also compared to the values of QuickScat observations.

The assessment of AMIP daily precipitations indicated that the values were too high. We decided to use then CMAP monthly climatological values, due to the lack of other data sources that could cover the RR time period.

The HadSST1 data set was evaluated versus the reference Mediterranean product and its quality enabled the surface heat flux correction procedure to be maintained, based on the difference between modeled and observed SST. The SST relaxation constant was calibrated and the value chosen ensure good results, as shown in D1.3.4.

A localization technique was implemented in the *OceanVar* data assimilation scheme to prevent spurious overshootings in the correction fields, far from observation locations. Basin mean RMSE and BIAS indices did not show much improvement while a local analysis and comparison of known circulation structures indicated that the localization procedures gave more consistent circulation patterns. We decided then to include the localization operator in the RR analysis scheme.

References

ADANI M., DOBRICIC S. , PINARDI N., 2011: Quality Assessment of a 1985–2007 Mediterranean Sea Reanalysis. *J. Atmos. Oceanic Technol*., 28, 569–589.
doi: http://dx.doi.org/10.1175/2010JTECHO798.1.

CHERCHI A. and A. NAVARRA, 2007: Sensitivity of the Asian summer monsoon to the horizontal resolution: differences between AMIP-type and coupled model experiments. *Climate Dynamics*, 28, 2, 273-290, doi: 10.1007/s00382-006-0183-z.

DEE D. P., S. M. UPPALA, A. J. SIMMONS, P. BERRISFORD, P. POLI, S. KOBAYASHI, U. ANDRAE et AL.: The ERA Interim reanalysis: configuration and performance of the data assimilation system. *Quarterly Journal of the Royal Meteorological Society* 137, no. 656 (2011): 553-597.

DOBRICIC S., PINARDI N., 2008: An oceanographic three-dimensional variational data assimilation scheme. *Ocean Modelling*, Volume 22, Issues 3–4, Pages 89-105, ISSN 1463-5003, 10.1016/j.ocemod.2008.01.004.

GATES,WL, 1992. AMIP: the atmosphere model intercomparison project. *Bulletin of American Meteorological Society* 73, 1962–1970.

KILLWORTH P. D.: Time interpolation of forcing fields in ocean models. *J. Phys. Oceanogr*., 26, 136–143, 1996.

MAILLARD C., and COAUTHORS, 2005: MEDAR/MEDATLAS 1998-2001: A Mediterranean and Black Sea oceanographic data base and network. *Boll. Geofis. Teor. Appl*., 46, 329–344.

MADEC G., P. DELECLUSE, M. IMBARD, and C. LEVY, 1998: OPA 8.1 ocean general circulation model reference manual. *Institut Pierre-Simon Laplace, Note du Pole de Modelisazion*, No. 11, 91 pp.

ODDO P., ADANI M., PINARDI N., FRATIANNI C., TONANI M., AND PETTENUZZO D., 2009: A nested Atlantic- Mediterranean Sea general circulation model for operational forecasting. *Ocean Sci.,* 5, 461–473.

PETTENUZZO D., W. G. LARGE, and N. PINARDI: On the corrections of ERA‐40 surface flux products consistent with the Mediterranean heat and water budgets and the connection between basin

surface total heat flux and NAO. *Journal of Geophysical Research: Oceans* (1978–2012) 115.C6 (2010).

RAYNER N. A., PARKER D. E., HORTON E. B., FOLLAND C. K., ALEXANDER L. V., ROWELL D. P., KENT E. C.KAPLAN, A. (2003): Global analyses of sea surface temperature, sea ice, and night marine air temperature since the late nineteenth century. *J. Geophys. Res.Vol.* 108, No. D14, 4407 10.1029/2002JD002670.

A.R. ROBINSON, M. GOLNARAGHI, W.G. LESLIE, A. ARTEGIANI, A. HECHT, E. LAZZONI, A. MICHELATO, E. SANSONE, A. THEOCHARIS, Ü. ÜNLÜATA: The eastern Mediterranean general circulation: features, structure and variability. *Dynamics of Atmospheres and Oceans, Volume* 15, Issues 3–5, April 1991, Pages 215-240, ISSN 0377-0265, 10.1016/0377-0265(91)90021-7.

TONANI M., PINARDI N., DOBRICIC S., PUJOL I., and FRATIANNI C., 2008: A high-resolution free-surface model of the Mediterranean Sea. *Ocean Sci*., 4, 1-14, doi:10.5194/os-4-1-2008.

UPPALA S.M., KÅLLBERG P.W., SIMMONS A.J., ANDRAE U., DA COSTA BECHTOLD V., FIORINO M., GIBSON J.K., HASELER J., HERNANDEZ A., KELLY G.A., LI X., ONOGI K., SAARINEN S., SOKKA N., ALLAN R.P., ANDERSSON E., ARPE K., BALMASEDA M.A., BELJAARS A.C.M., VAN DE BERG L., BIDLOT J., BORMANN N., CAIRES S., CHEVALLIER F., DETHOF A., DRAGOSAVAC M., FISHER M., FUENTES M., HAGEMANN S., HÓLM E., HOSKINS B.J., ISAKSEN L., JANSSEN P.A.E.M., JENNE R., MCNALLY A.P., MAHFOUF J.-F., MORCRETTE J.-J., RAYNER N.A., SAUNDERS R.W., SIMON P., STERL A., TRENBERTH K.E., UNTCH A., VASILJEVIC D., VITERBO P., and WOOLLEN J. 2005: The ERA-40 re-analysis. *Quart. J. R. Meteorol. Soc*., 131, 2961-3012.doi:10.1256/qj.04.176.15.

XIE P., and P.A. ARKIN, 1997: Global precipitation: a 17-year monthly analysis based on gauge observations, satellite estimates, and numerical model outputs. *Bull. Amer. Meteor. Soc*., 78, 2539 - 2558.